

The Relationship Between High-Order Aberration and Anterior Ocular Biometry During Accommodation in Young Healthy Adults

Bilian Ke,^{1,2} Xinjie Mao,^{2,3} Hong Jiang,² Jichang He,⁴ Che Liu,² Min Li,¹ Ying Yuan,¹ and Jianhua Wang²

¹Department of Ophthalmology, Shanghai General Hospital, Shanghai Jiao Tong University School of Medicine, Shanghai, China

²Bascom Palmer Eye Institute, University of Miami Miller School of Medicine, Miami, Florida, United States

³School of Ophthalmology and Optometry, Wenzhou Medical University, Wenzhou, China

⁴New England College of Optometry, Boston, Massachusetts, United States

Correspondence: Jianhua Wang, Bascom Palmer Eye Institute, University of Miami, Miller School of Medicine, 1638 NW 10th Avenue, McKnight Building, Room 202A, Miami, FL 33136, USA; jwang3@med.miami.edu.

Submitted: February 22, 2017

Accepted: October 2, 2017

Citation: Ke B, Mao X, Jiang H, et al. The relationship between high-order aberration and anterior ocular biometry during accommodation in young healthy adults. *Invest Ophthalmol Vis Sci.* 2017;58:5628–5635. DOI: 10.1167/iops.17-21712

PURPOSE. This study investigated the anterior ocular anatomic origin of high-order aberration (HOA) components using optical coherence tomography and a Shack-Hartmann wavefront sensor.

METHODS. A customized system was built to simultaneously capture images of ocular wavefront aberrations and anterior ocular biometry. Relaxed, 2-diopter (D) and 4-D accommodative states were repeatedly measured in 30 young subjects. Custom software was used to correct optical distortions and measure biometric parameters from the images.

RESULTS. The anterior ocular biometry changed during 2-D accommodation, in which central lens thickness, ciliary muscle thicknesses at 1 mm posterior to the scleral spur (CMT1), and the maximum value of ciliary muscle thickness increased significantly, whereas anterior chamber depth, CMT3, radius of anterior lens surface curvature (RAL), and radius of posterior lens surface curvature (RPL) decreased significantly. The changes in the anterior ocular parameters during 4-D accommodation were similar to those for the 2-D accommodation. Z_4^0 decreased significantly during 2-D accommodation, and Z_3^{-1} , Z_3^1 , Z_4^0 , and Z_6^0 shifted to negative values during 4-D accommodation. The change in Z_4^0 negatively correlated with those in CMT1, and the negative change in Z_3^1 correlated with changes in RAL and CMT1.

CONCLUSIONS. HOA components altered during step-controlled accommodative stimuli. Ciliary muscle first contracted during stepwise accommodation, which may directly contribute to the reduction of spherical aberration (SA). The lens morphology was then altered, and the change in anterior lens surface curvature was related to the variation of coma.

Keywords: optical coherence tomography, wavefront aberration, ciliary muscle, anterior ocular biometry

Accommodation is a dynamic process in which the optical apparatus in human eyes changes and adjusts.¹ The purpose of accommodation is to obtain a clear image on the retina. Low-order aberrations (LOAs) and high-order aberrations (HOAs) change to compensate for the defocus of the retina as a function of accommodation.² Ocular anterior segment alters significantly during accommodation, which can secondarily cause the change in aberrations. The classic accommodative theory of Helmholtz³ states that the ciliary muscle contracts when accommodation occurs; in turn, radius of curvature of the lens decreases and lens thickness increases, which leads to the changes in refractive power and brings objects into focus on the retina.

Many studies have been conducted to better understand the changes of accommodation apparatus and aberration during accommodation.^{4–9} Shi et al.⁴ investigated ocular anterior segment biometry and aberrations by combining optical coherence tomography (OCT) and Shack-Hartmann wavefront sensors, but they did not capture the image of ciliary muscle, which is supposed to be the core point of accommodation.

Yuan et al.⁵ declared that the increase in HOAs was primarily due to increased convexity of the anterior surface of the lens during accommodation. Smith et al.⁶ demonstrated that spherical aberration (SA) was affected by lens surface curvature and refractive index in a model eye. Our previous study recorded the dynamic procedures of ciliary muscles during accommodation using a synchronized SD-OCT system.⁷ The Schachar theory also anticipated the changes of ciliary muscle during accommodation,⁸ and the force of ciliary muscle reduced with the increasing of age, involved in the change of accommodation related with presbyopia.⁹

The Helmholtz theory of accommodation does not assert that the peripheral surface of the lens becomes flattened during accommodation.¹⁰ In contrast, the Schachar theory proposes that the flattening of the crystalline lens periphery during accommodation results in a shift in SA in the negative direction.¹¹ The negative shift of SA has been demonstrated in a series of studies.^{12–18} However, none of these studies accounted for changes in ocular anterior segment biometry including ciliary muscle combined with wavefront aberrations



during accommodation. Also the stepwise change of HOA components during step-controlled accommodation stimuli still remains unclear.

A variety of imaging techniques, such as ultrasound biomicroscopy (UBM), magnetic resonance imaging (MRI), Scheimpflug photography, and more recently OCT, were developed to measure dimension changes during accommodation.¹⁹⁻²¹ However, it is difficult to define interactions between components because of limitations of the instrument. For example, a previous study⁵ found that HOAs increased during in vivo accommodative stimuli. However, the accommodative response was measured from the test eye while stimulus was presented to the contralateral eye. This paradigm suffers from measurement errors because of asynchronies between the two eyes. The classic accommodative mechanism was based on the concept that the contraction of the ciliary muscle is the initial event in the process of accommodation, and it also induced changes in ocular wavefront aberrations. Change in HOAs seems to be important because it influences retinal image quality, which is thought to play an important role in the progression of myopia.²² Other studies^{5,23} used combinations of two OCTs or anterior OCT with a wavefront sensor to quantify accommodative changes with aberrations; to our knowledge, no previous reports analyzed gradient changes of HOA components and anterior ocular biometry, including ciliary muscles during step-controlled stimuli of accommodation. To better understand the underlying regulatory mechanisms of accommodation, we built a customized system that synchronized ultra-long scan depth OCT, ciliary muscle (CM)-OCT, and Shack-Hartmann wavefront sensor integrated with a Badal system aimed at examining the dynamic relationship between anterior ocular biometric factors including ciliary muscles and optical changes, especially the HOAs, using in vivo step-controlled accommodative stimuli.

MATERIALS AND METHODS

Apparatus

We built a customized slit-lamp platform that combined three sample arms together. The complementary metal-oxide semiconductor (CMOS)-OCT and CM-OCT probes were mounted on the platform with the Shack-Hartmann wavefront sensor probe. A Badal system was added to the wavefront sensor channel to stimulate and capture the accommodative response simultaneously (Fig. 1).

The ultra-long scan depth spectral-domain OCT (SD-OCT) with CMOS was set up as previously reported.^{7,24-28} The CMOS-OCT in this synchronic system was equipped with four mirrors and can be used to get a full eye image, and the details of imaging the full eye were provided in our previous studies.²⁴⁻²⁷ In the present study, a switchable reference arm with two mirrors was used, and the anterior segment from the cornea to the back of the crystalline lens was imaged.^{7,28} The scan depth of the spectrometer was 12.57 mm in air. As detailed in our previous study,²⁸ the difference (11 mm) in the optical pathway distance between two mirrors resulted in placing the zero-delay lines of the two images on the top and the bottom. Overlapping these two images, the sensitivity drop versus the depth was compensated. The iris image in both images was used to register both images for overlapping. The CMOS-OCT had the following features: 70,000 A-lines/speed, 12.57-mm scan depth in air, 840-nm central wavelength, 50-nm bandwidths, 1.11-mW output power, and 7.7- μ m axial resolution in air.

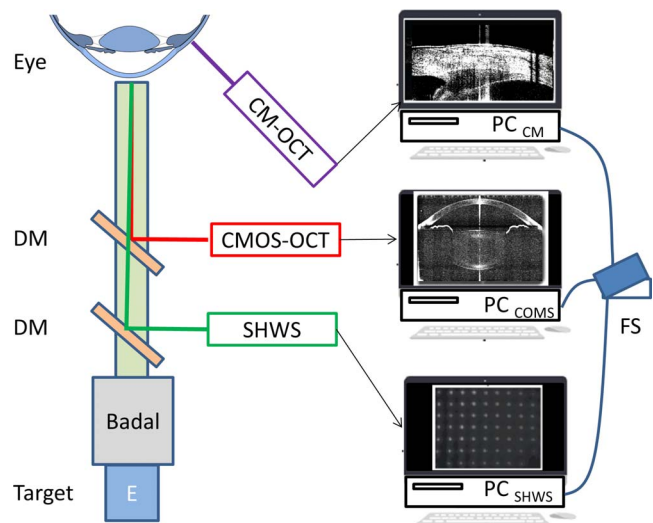


FIGURE 1. Schematic diagram of the synchronic system including the combined OCT systems and the Shack-Hartmann wavefront sensor. CM-OCT, ciliary muscle OCT; CMOS-OCT, complementary metal-oxide semiconductor OCT; SHWS, Shack-Hartmann wavefront sensor; DM, dichroic mirror; PC, personal computer; FS, footswitch.

Another SD-OCT (CM-OCT) was used to image the ciliary muscle, as previously described in detail.²⁸ The CM-OCT had the following features: the superluminescent diode (SLD) light source centered at a 1310-nm wavelength, 75 nm for full width at half-maximum bandwidths; the output power was 2.6 mW, and the axial resolution was 8.0 μ m in air. The CM-OCT captures seven frames per second with 1000 A-lines per frame with the depth of 3.8 mm. An electronic shutter (JML Optical, Rochester, NY, USA) was implanted in the reference arm to insert a synchronized signal into the real-time image-acquiring video. The Shack-Hartmann wavefront sensor had the following features: wavelength of 750 nm, bandwidth of 25 nm, and output power of 0.20 mW. The distorted wavefront aberration of the eye was balanced using a 10 \times 10 microlens array (Edmund Optics, Barrington, NJ, USA) and captured using a CCD camera (Uniq Vision, Santa Clara, CA, USA). The focal length and dimension of each microlens was 32.8 mm and 0.5 mm \times 0.5 mm. The image-acquiring speed of the camera was 60 frames per second, which was controlled by customized software based on C Programming Language (American National Standard Institute, ANSI). A black slide with different "Snellen E" sizes served as the visual target. A movable lens (Thorlabs, Newton, NJ, USA) conjugated with the visual target in the Badal system was used to provide the stepwise accommodative stimuli. The schematic of this synchronic system was reported in our previous study²⁶ and is illustrated in Figure 1.

This study prealigned these three systems prior to the test to ensure that the images would be captured at the same position and simultaneously. First, the CMOS-OCT and CM-OCT probes were mounted on the slit-lamp. The Shack-Hartmann wavefront sensor probe was also mounted for combination with the OCT systems. The apexes of the horizontal and vertical frames via CMOS-OCT cross-session scanning were used to align the eye location. The apex of the CM-OCT system was aligned with the CMOS-OCT system at the same position. The beam of the Shack-Hartmann wavefront sensor was centrally prealigned with the CMOS-OCT system before the experiment. The apexes of CMOS-OCT vertical and horizontal scans were used to align the eye location during the test.

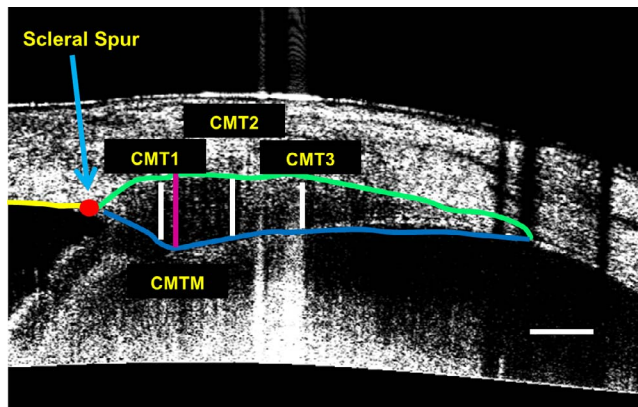


FIGURE 2. The measurements of the ciliary muscle. The image was optically corrected following Snell's principle; CMT1 through CMT3, the thickness of the ciliary muscle at 1, 2, and 3 mm posterior to the scleral spur. CMTM, the maximum thickness of the ciliary muscle. Scale bar: 1 mm.

Participants

Thirty healthy adults (12 males and 18 females, mean age 31.1 ± 6.8 years) were enrolled in this study. The mean spherical equivalent (SE) was -2.28 diopters (D) (range, 0 to -6.00 D). People over 40 years old with an SE greater than -6.00 D were excluded. All subjects were normal in ophthalmic examination and had no history of systemic diseases. This study complied with the tenets of the Declaration of Helsinki, and the institutional review board for human research at the University of Miami approved the study. Informed consent was obtained from each subject prior to participation.

Procedure

Measurements were performed with the room lights off. Subjects were asked to sit in front of the system with their chin resting on the platform and forehead touching the band. We adjusted the Badal system to reach the subject's far point at the beginning.² A black "Snellen E" was printed on glazed transparent paper as the visual target. The target was backlit using a miniature light-emitting diode (LED) bulb covered with a piece of white diffuse fiber. Subjects were asked to watch the fixation target "E" with the examined eye while the other eye was patched. We pushed the Badal system forward to induce 2- and 4-D accommodation while the subject focused on the same target to keep it as clear as possible. When the subject was looking at the fixation target during accommodation, the apex of the cornea was relocated from the horizontal and vertical scans of the CMOS-OCT and the pupil was centered to the CMOS-OCT and Shack-Hartman wavefront sensor. The synchronized system simultaneously captured the CMOS-OCT, CM-OCT, and wavefront sensor images under natural pupils. The entire procedure was repeated after a 5-minute break.

Image Processing and Data Analysis

The image analysis methods for CMOS-OCT and CM-OCT complied with those in our previous published paper.^{22,23} Two images obtained using CMOS-OCT were registered using the iris and were overlaid. After that, the boundaries of the cornea and the crystalline lens were semiautomatically outlined using custom software, which performed optical correction based on Snell's principle as detailed in our previous studies.^{23,28} A series of refractive indexes were used, and the details can be found in a previous paper.⁷ Data of CT, anterior chamber depth (ACD), central lens thickness (CLT), radius of anterior lens

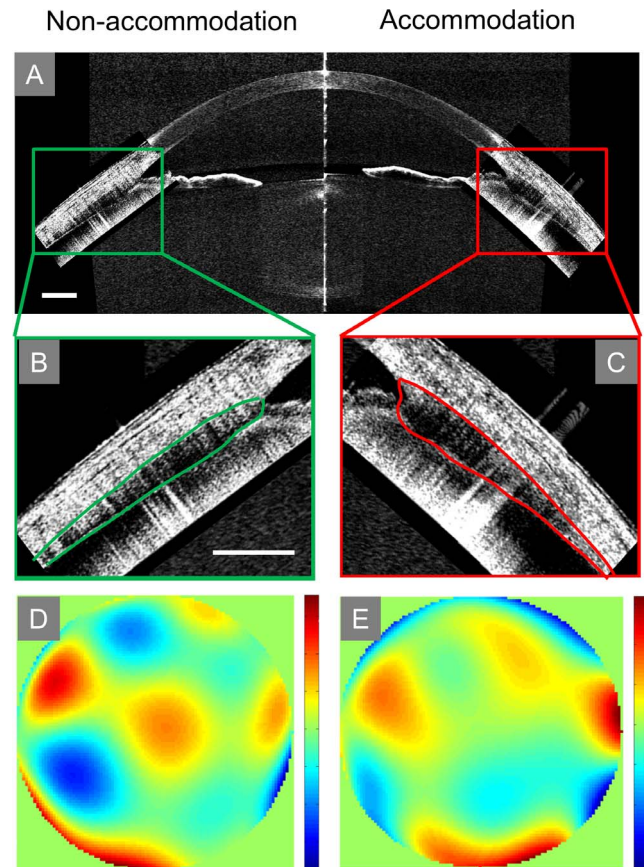


FIGURE 3. Typical images of anterior ocular biometry and wavefront aberration before and after accommodation. (A) Anterior ocular biometry images of nonaccommodation status using CMOS-OCT and CM-OCT. The *left side* of the image (horizontally flipped for illustration purposes) was at nonaccommodation status, and the *right side* of the image was at accommodation status. (B) Ciliary muscle at nonaccommodation status. (C) Ciliary muscle at accommodation status. Note that all images (A–C) were optically corrected. (D) Higher-order aberration image of nonaccommodation status. (E) Higher-order aberration image of 4-D accommodation stimulus status. Scale bars: 1 mm.

surface curvature (RAL), and radius of posterior lens surface curvature (RPL) were calculated from the CMOS-OCT images.

To enhance the image of the ciliary muscle, three ciliary muscle images from the video of each accommodative state were separately superimposed, registered, and averaged. The enhanced ciliary muscle image of the different accommodative states was then compared for analysis.²⁸ Ciliary muscle thicknesses at 1 mm (CMT1), 2 mm (CMT2), and 3 mm (CMT3) posterior to the scleral spur and the maximum value of ciliary muscle thickness (CMTM) were obtained from the averaged CM-OCT images (Fig. 2).²⁸

The Shack-Hartmann images of 9×9 points were analyzed using custom-developed code.¹⁴ The coefficients of seven-order Zernike polynomials, including 35 terms, were obtained at the 4-mm-diameter pupil area. We calculated the root mean square (RMS) of LOAs, HOAs, and the Zernike coefficients of coma (Z_3^{-1} , Z_3^1 , Z_5^{-1} , Z_5^1), and SA (Z_4^0 , Z_6^0) under 0.00-, 2-, and 4-D accommodative stimuli. SA was calculated as the RMS of the sum of the squared coefficients of Z_4^0 and Z_6^0 .²⁹ The average value of five wavefront images, which were captured in one synchronized procedure, was used to estimate the wavefront aberration status. HOAs were transformed into color-coded maps using custom Matlab code (MathWorks, Natick, MA, USA) (Fig. 3).

TABLE 1. The Anterior Ocular Biometry of Baseline (0 D) and Accommodation Stations (2 D, 4 D) in 30 Subjects, mm

Measures	0 D	2 D	4 D
CCT	0.5422 ± 0.0302	0.5420 ± 0.0290	0.5422 ± 0.0292
ACD	3.1672 ± 0.2964	3.0981 ± 0.2925*	3.0073 ± 0.2894*
PD	5.3081 ± 0.7947	4.9394 ± 0.8238	4.3845 ± 0.7588
Crystalline lens			
RAL	11.9453 ± 1.6895	10.3770 ± 1.7058*	8.7877 ± 1.3575*
RPL	6.1151 ± 0.7720	5.4226 ± 0.7600*	4.8558 ± 0.7272*
CLT	3.8011 ± 0.2551	3.8852 ± 0.2515*	3.9857 ± 0.2713*
Ciliary muscle			
CMT1	0.5721 ± 0.0604	0.6755 ± 0.0726*	0.7616 ± 0.0925*
CMT2	0.4526 ± 0.0931	0.4626 ± 0.1283	0.4480 ± 0.1229
CMT3	0.2785 ± 0.0712	0.2443 ± 0.0805*	0.2151 ± 0.0696*
CMTM	0.5951 ± 0.0629	0.7030 ± 0.0719*	0.7881 ± 0.0930*

* Significant *P* value analyzed by 1-way ANOVA, *P* < 0.05 (2 vs. 0 D and 4 vs. 0 D).

The measurement results of the two image sessions were averaged. Statistical analyses were performed to compare the parameters at each stepwise accommodative state.

RESULTS

Repeatability of Anterior Ocular Biometry and Wavefront Aberration

Repeated measurements were performed in all subjects in this study. There were no differences between the two repeated measurements of the same accommodative state for anterior ocular parameters and wavefront aberrations (*P* > 0.05). We determined whether differences existed between two states using the average of the two measurements for each accommodative state. The coefficients of repeatability (CORs) for central corneal thickness (CCT), ACD, CLT, CMT1, CMT2, CMT3, and CMTM ranged from 0.013 to 0.193 in the different accommodative states. The percentage of CORs (CORs%) ranged from 0.48% to 17.24%. The CORs of Z_3^{-1} , Z_3^1 , Z_4^0 , Z_5^{-1} ,

Z_5^1 , Z_6^0 LOA and HOA were also excellent and ranged from 0.016 to 0.112. The CORs of RAL and RPL ranged from 1.428 to 2.372, but the CORs% were relatively high, ranging from 17.85% to 29.41%.

Accommodative Changes of Anterior Ocular Biometry

As observed in our previous study there was definite notching of the anterior radial muscle fibers of the ciliary muscle during accommodation (Fig. 3).^{7,8} Overall, ACD, RAL, RPL, and CMT3 decreased significantly, and CLT, CMT1, and CMTM increased significantly during 2- and 4-D accommodation. ACD decreased significantly during accommodation, which may be due to the increase in CLT. RAL and RPL declined simultaneously, whereas CLT increased significantly. CMT1 and CMTM exhibited a significant rising trend, whereas CMT3 exhibited a minor decrease. Taken together, the direction of changes during 4-D accommodation was similar to 2-D accommodation, while the degree of changes was more pronounced in 4-D stage. CCT and CMT2 remained unchanged during stepwise accommodative stimuli (Table 1; Fig. 4).

Changes in Wavefront Aberration Components During Accommodation

Low-order RMS (LORMS) increased significantly during the 2-D accommodation, and it continued to rise during the 4-D stage. For HOA components, in the 2-D stage, firstly Z_4^0 and SA decreased remarkably. During the 4-D stage, Z_4^0 and Z_6^0 had more profound reductions, and then shifted to negative status. Z_3^{-1} , Z_3^1 and coma were found to have significant differences at the 4-D stage compared to the 0-D stage (Table 2; Fig. 5).

Relationship Between Anterior Ocular Biometry and Wavefront Aberration Components During Stepwise Accommodation

Pearson correlation analysis was used to determine the relationship between anterior ocular biometry and wavefront

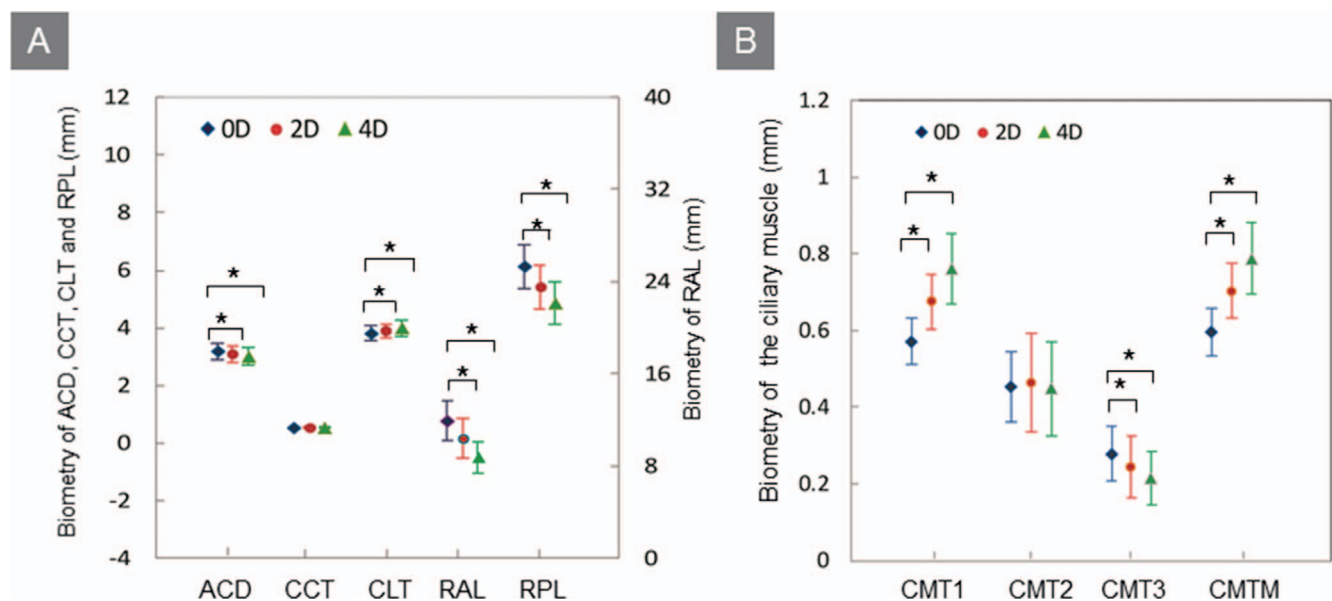


FIGURE 4. Analysis of changes in anterior ocular biometry under baseline (0 D) and accommodation stations (2 D, 4 D) using CMOS-OCT and CM-OCT. Entire eye images in 30 subjects were recorded using CMOS-OCT without or with accommodation (2 D, 4 D). Ciliary muscle images of 30 subjects were recorded using CM-OCT without or with accommodation (2 D, 4 D). **P* < 0.05.

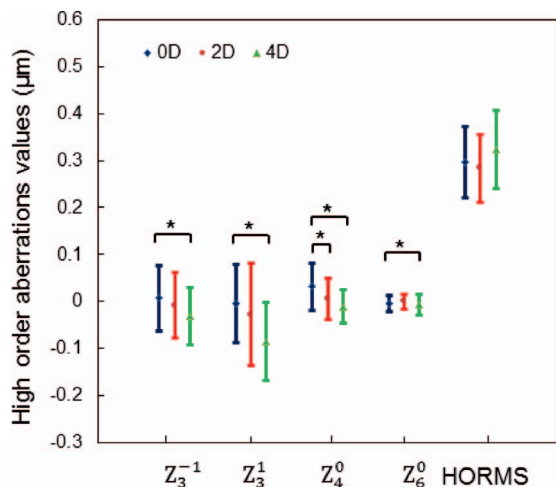


FIGURE 5. Wavefront aberrations of baseline (0 D) and accommodation station (2 D, 4 D) using the Shack-Hartmann wavefront sensor. Changes in wavefront aberration were recorded in 30 subjects using the Shack-Hartmann wavefront sensor without or with accommodation. * $P < 0.05$.

aberration components. The changes in Z_4^0 and SA negatively correlated with CMT1 and CMTM under 2-D accommodation (Fig. 6), and the changes in Z_3^1 and coma negatively correlated to the change in RAL under 4-D accommodation (Fig. 7). The change of Z_2^0 had a significant negative relationship with the change of pupillary diameter (PD) under 2-D accommodation compared to 0-D station. The change of Z_4^0 had a significant positive relationship with the change of PD under 4-D accommodation compared to 0 D (Fig. 8).

DISCUSSION

Accommodation is a dynamic optical performance, during which the crystalline lens increases its curvature and thickness to increase the dioptric power due to contraction of the ciliary muscle.^{30,31} Our study focused on the components of the optical apparatus allows a better understanding of the anatomic origin of wavefront aberrations during accommodation. We investigated the sequential change of HOA components and its relationship with anterior ocular biometry using a customized three-in-one system. Some previous studies concerned the relationship during ocular anterior segment

TABLE 2. Wavefront Aberrations of Baseline (0 D) and Accommodation Station (2 D, 4 D) in 30 Subjects; Based on 4-mm Pupil Size, mm

Wavefront Aberration	0 D	2 D	4 D
LORMS	0.4834 ± 0.2335	0.6622 ± 0.2564*	0.7837 ± 0.2631*
HORMS	0.2960 ± 0.0755	0.2833 ± 0.0728	0.3232 ± 0.0824
Z_3^{-1}	0.0068 ± 0.0707	-0.0083 ± 0.0698	-0.0306 ± 0.0609*
Z_3^1	-0.0037 ± 0.0825	-0.0277 ± 0.1097	-0.0851 ± 0.0836*
Z_5^{-1}	-0.0013 ± 0.0240	-0.0022 ± 0.0311	-0.0023 ± 0.0281
Z_5^1	-0.0135 ± 0.0366	-0.0152 ± 0.0245	-0.0025 ± 0.0517
Coma	0.1003 ± 0.0597	0.1243 ± 0.0602	0.1377 ± 0.0550**
Z_4^0	0.0314 ± 0.0491	0.0054 ± 0.0439*	-0.0109 ± 0.0356*
Z_6^0	-0.0050 ± 0.0170	-0.0003 ± 0.0150	-0.0075 ± 0.0222*
SA	0.0508 ± 0.0328	0.0403 ± 0.0223*	0.0360 ± 0.0246

* $P < 0.05$ analyzed by 1-way ANOVA (2 D vs. 0 D and 4 D vs. 0 D).
 ** $P < 0.01$ analyzed by 1-way ANOVA (2 D vs. 0 D and 4 D vs. 0 D).

biometry, HOAs, or other elements with accommodation (Table 3); however, none of these measured the change of anterior segment including ciliary muscle along with the change of HOA components using stepwise accommodation stimuli. Compared to our previous study, one of the most important advancements applied in this study lies in the measurement range of wavefront system. Here we use a Badal system up to 10.0 D in which the inside visual target enables us to add 4-D stimuli even for the -6.0-D subjects. To the best of our knowledge, this study is the first to demonstrate the component change of HOAs and its relationship to the anterior ocular biometry parameters under accommodation stimuli.

The Sequential Change of HOA Components During 2- and 4-D Accommodation Stimuli

Notably, we found that the changes in HOA component obeyed an accommodation-dependent and wavefront Zernike order-dependent sequence. The amount of SAs Z_4^0 and Z_6^0 declined with 2-D stimuli ($P < 0.01$), and the coma (Z_3^{-1} , Z_3^1 , Z_5^{-1} , Z_5^1) exhibited a slight shift to the negative ($P > 0.05$). The Z_4^0 and Z_6^0 became more negative when the accommodation stimulus increased to 4 D ($P < 0.01$). The coma Z_3^{-1} , Z_3^1 significantly decreased ($P < 0.01$), but the second-order coma (Z_5^{-1} , Z_5^1) exhibited no significant change ($P > 0.05$). HOAs likely exhibit their own inner change order during accommodation. SA and coma are optical defects, which affect the image quality of the eye.^{32,33} Previous studies^{16,34} demonstrated that a strong

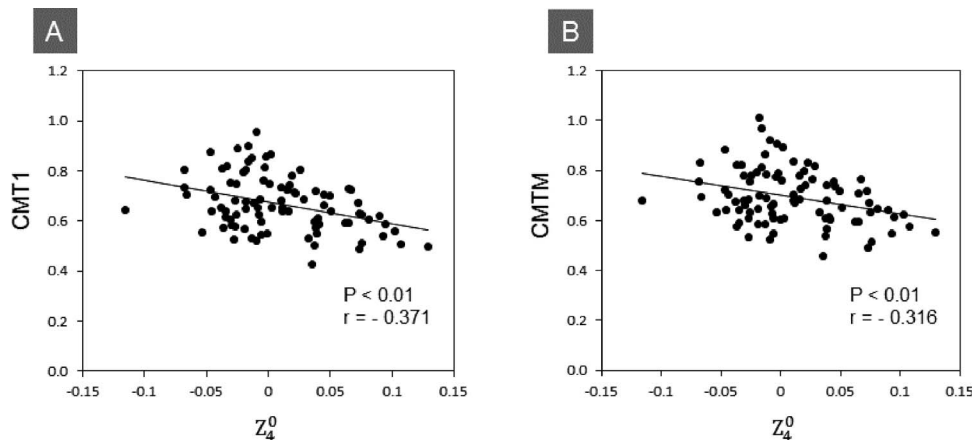


FIGURE 6. Correlations between changes in spherical aberration and changes in anterior ocular biometry. The change in Z_4^0 exhibited a significant negative relationship with CMT1 and CMTM under 2-D accommodation compared to the baseline (0-D) station.

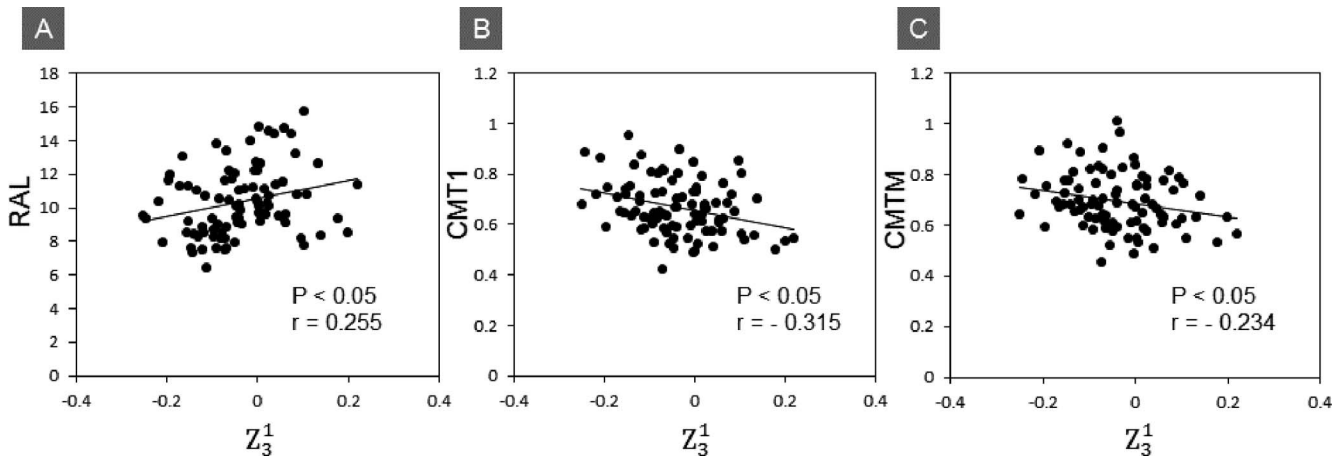


FIGURE 7. Correlations between changes in coma and changes in anterior ocular biometry. The change in Z_3^1 exhibited a significant positive relationship with RAL under 4-D accommodations compared to the baseline (0-D) station, and the change in Z_3^1 exhibited a significant negative relationship with CMT1 and CMTM under 4-D accommodations.

negative SA in a relaxed eye exacerbated myopia progression. It was also reported that increased aberrations decreased optical acuity.³⁵ It was widely considered that close distance can invoke strong accommodation, and near work has a close relationship with myopia. However, the underlying mechanism of how near work affects myopia progression is not known. Many people^{16,36,37} believed that inaccurate accommodation caused retinal blur image, which would promote eyeball growth. We found that SA shifted to negative when accommodative stimuli gradually increased. A negative SA is the combination leading to relatively low contrast in the defocused retinal image.¹⁶ We also found that the impact of HOAs on optical quality increased by the stepwise accommodation, which resulted from the additional changes in coma when 4-D accommodation was given. Near work creates an overaccommodation and may disturb the influence of HOAs on elaborate optical quality, which may contribute to myopia eventually.

The Relationship Between HOA Components and Anterior Ocular Biometry

Our results demonstrated that Z_4^0 and total SA exhibited great correlation with CMT1 and CMTM, which means that contraction of the ciliary muscle triggers the change in SA

first. Z_3^1 and total coma correlated with CMT2, CMT3, and RAL. The contraction of ciliary muscle induces changes in lens curvature on the anterior and posterior surface, and the change of anterior surface was much more remarkable than that of the posterior surface.²³ SA may be induced first at lower degrees of accommodation, but the change in coma does not appear until the RAL changes distinctly. Coma is the Zernike polynomial term for one of the third-order aberrations, and SA is the Zernike polynomial term for one of the more significant fourth-order aberrations. Parallel light rays from infinity are refracted into a spherical wavefront during emmetropias, which in proper order converges to a pinpoint focus on the retina. This sophisticated physiological process is likely mutilated by coma and SA. Very few studies investigated the correlation between HOAs and ocular biometry. Our study found a negative relationship between the changes in SA and ciliary muscles when accommodation appeared. The change of coma negatively correlated with anterior lens surface curvature. Ciliary muscle may provide the original power of the eye biometry change. Therefore, ciliary muscle thickness significantly contributes to the production of SA and coma, which affects SA first. With increasing accommodation, ciliary muscle thickness changed more obviously followed by the change of radius curvature of the lens. In general, the ciliary muscle plays

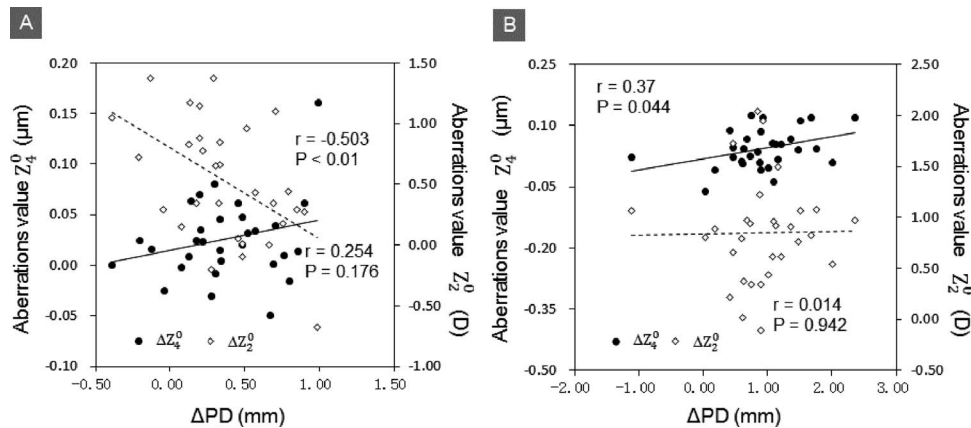


FIGURE 8. Correlations between the change of pupillary diameter (PD) and the change of Z_2^0 or Z_4^0 at 2- and 4-D accommodations compared with the baseline station (0 D). (A) 0 vs. 2 D; (B) 0 vs. 4 D. ΔPD , pupillary diameter (2 or 4 D) – pupillary diameter (0 D), $\Delta Z_2^0 = Z_2^0$ (2 or 4 D) – Z_2^0 (0 D), $\Delta Z_4^0 = Z_4^0$ (2 or 4 D) – Z_4^0 (0 D). The change of Z_4^0 had a significant negative relationship with the change of PD under 2-D accommodation compared to 0-D station. The change of Z_4^0 had a significant positive relationship with the change of PD under 4-D accommodation compared to 0-D station.

TABLE 3. Research on Ocular Anterior Segment Biometry and Other Elements During Accommodation

Authors	Measurement	Sample Size	Device	Conclusions
Shi et al. ⁴	Ocular anterior segment dimension parameters and HOAs	/	UL-SD-OCT and a Shack-Hartmann wavefront sensor	The system could record the ocular anterior parameters and HOAs with accommodative stimuli.
Yuan et al. ⁵	Ocular anterior segment biometry and HOAs	35	Combined UL-OCT and wavefront sensor	The anterior segment biometry and the HOAs changed significantly during accommodation.
Shao et al. ⁷	Anterior segment including ciliary muscle and age	33	Synchronized SD-OCT system	Age-related changes in the lens reshaping and ciliary muscle forward movement were found.

UL, ultra-long.

a role during accommodation, and it is the physiological origin of wavefront aberration changes.

There are some limitations in this study. Due to the attenuation of the OCT light, the ciliary muscle image based on OCT may not be as clear as the image obtained by UBM.³⁸ However, we averaged the superimposition of three images of the ciliary muscle from the videos of each accommodative state to enhance the image of the ciliary muscle. This may have increased the variability of the accommodative change in ciliary muscle thickness. Since the analyzing software was not fully automated and adjustments were performed manually, additional variability may have occurred during all the measurements.

Retinal OCT studies use registration algorithms or rigid point-based registration for image registration.^{39,40} Our anterior segment study did not use these methods due to the complexity of our combined system. We imaged the fixating eye; however, even with monocular fixation, the eye cyclotorts during accommodation.^{41,42} Although we used the corneal apex to align the CMOS-OCT, this did not correct for eye rotational shifts. We aligned the CMOS-OCT and Shack-Hartmann wavefront sensor with the center of the pupil. Since the pupil is known to shift with accommodation, this introduced an additional nonrandom variable. These nonrandom variables may have resulted in distortion of the images and/or exaggeration of the measured changes.

In conclusion, SD-OCT and CM-OCT combined with the Shack-Hartmann sensor successfully measured the accommodative changes in anterior ocular morphologic parameters including the ciliary muscle and wavefront aberrations. During stepwise accommodation, the anterior chamber became shallower, central lens thickness increased, and the anterior and posterior central lens surfaces steepened. Primary SA (Z_4^0) shifted negatively earlier than coma, and both were significantly related to the change in the ciliary muscle. With accommodation the increase in curvature of the anterior lens surface contributed to the change in coma. Future studies incorporating image registration with invariant positional references, objective measure of accommodation, pupillary dilation, and high-speed data acquisition with frame averaging may significantly improve the accuracy of the measurements.

Acknowledgments

Supported in part by Research Grants EY020607S, EY021336, National Institutes of Health Center Grant P30 EY014801, and Research to Prevent Blindness.

Disclosure: **B. Ke**, None; **X. Mao**, None; **H. Jiang**, None; **J. He**, None; **C. Liu**, None; **M. Li**, None; **Y. Yuan**, None; **J. Wang**, None

References

- Atchison DA. Accommodation and presbyopia. *Ophthalmic Physiol Opt.* 1995;15:255-272.
- He JC, Wang J. Measurement of wavefront aberrations and lens deformation in the accommodated eye with optical coherence tomography-equipped wavefront system. *Opt Express.* 2014;22:9764-9773.
- Harper DG. Bringing accommodation into focus: the several discoveries of the ciliary muscle. *JAMA Ophthalmol.* 2014;132:645-648.
- Shi G, Wang Y, Yuan Y, Wei L, Lv F, Zhang Y. Measurement of ocular anterior segment dimension and wavefront aberration simultaneously during accommodation. *J Biomed Opt.* 2012;17:120501.
- Yuan Y, Shao Y, Tao A, et al. Ocular anterior segment biometry and high-order wavefront aberrations during accommodation. *Invest Ophthalmol Vis Sci.* 2013;54:7028-7037.
- Smith G, Atchison DA, Iskander DR, Jones CE, Pope JM. Mathematical models for describing the shape of the in vitro unstretched human crystalline lens. *Vision Res.* 2009;49:2442-2452.
- Shao Y, Tao A, Jiang H, et al. Age-related changes in the anterior segment biometry during accommodation. *Invest Ophthalmol Vis Sci.* 2015;56:3522-3530.
- Schachar RA. Human accommodative ciliary muscle configuration changes are consistent with Schachar's mechanism of accommodation. *Invest Ophthalmol Vis Sci.* 2015;56:6075.
- Schachar RA. Dynamic aspects of accommodation: age and presbyopia. *Vision Res.* 2004;44:2313-2316.
- Fincham E. Mechanism of accommodation. *Br J Ophthalmol.* 1937;92(suppl):5-80.
- Schachar R, Cudmore D, Black T. A revolutionary variable focus lens. *Ann Ophthalmol.* 1996;28:11-18.
- Hazel CA, Cox MJ, Strang NC. Wavefront aberration and its relationship to the accommodative stimulus-response function in myopic subjects. *Optom Vis Sci.* 2003;80:151-158.
- Cheng H, Barnett JK, Vilupuru AS, et al. A population study on changes in wave aberrations with accommodation. *J Vis.* 2004;4(4):3.
- He JC, Burns SA, Marcos S. Monochromatic aberrations in the accommodated human eye. *Vision Res.* 2000;40:41-48.
- Fritsch M, Dawczynski J, Jurkutat S, Vollandt R, Strobel J. Monochromatic aberration in accommodation. Dynamic wavefront analysis [in German]. *Ophthalmologe.* 2011;108:553-560.
- Thibos LN, Bradley A, Liu T, Lopez-Gil N. Spherical aberration and the sign of defocus. *Optom Vis Sci.* 2013;90:1284-1291.
- Gwiazda JE, Hyman L, Norton TT, et al. Accommodation and related risk factors associated with myopia progression and their interaction with treatment in COMET children. *Invest Ophthalmol Vis Sci.* 2004;45:2143-2151.
- Zhou XY, Wang L, Zhou XT, Yu ZQ. Wavefront aberration changes caused by a gradient of increasing accommodation stimuli. *Eye (Lond).* 2015;29:115-121.
- de Castro A, Birkenfeld J, Maceo B, et al. Influence of shape and gradient refractive index in the accommodative changes

- of spherical aberration in nonhuman primate crystalline lenses. *Invest Ophthalmol Vis Sci.* 2013;54:6197-6207.
20. Dai C, Zhou C, Fan S, et al. Optical coherence tomography for whole eye segment imaging. *Opt Express.* 2012;20:6109-6115.
 21. Doyle L, Little JA, Saunders KJ. Repeatability of OCT lens thickness measures with age and accommodation. *Optom Vis Sci.* 2013;90:1396-1405.
 22. Hiraoka T, Kakita T, Okamoto F, Oshika T. Influence of ocular wavefront aberrations on axial length elongation in myopic children treated with overnight orthokeratology. *Ophthalmology.* 2015;122:93-100.
 23. Du C, Shen M, Li M, Zhu D, Wang MR, Wang J. Anterior segment biometry during accommodation imaged with ultra-long scan depth optical coherence tomography. *Ophthalmology.* 2012;119:2479-2485.
 24. Zhong J, Shao Y, Tao A, et al. Axial biometry of the entire eye using ultra-long scan depth optical coherence tomography. *Am J Ophthalmol.* 2014;157:412-420.
 25. Zhong J, Tao A, Xu Z, et al. Whole eye axial biometry during accommodation using ultra-long scan depth optical coherence tomography. *Am J Ophthalmol.* 2014;157:1064-1069.
 26. Mao X, Banta JT, Ke B, et al. Wavefront derived refraction and full eye biometry in pseudophakic eyes. *PLoS One.* 2016;11:e0152293.
 27. Tao A, Shao Y, Zhong J, Jiang H, Shen M, Wang J. Versatile optical coherence tomography for imaging the human eye. *Biomed Opt Express.* 2013;4:1031-1044.
 28. Shao Y, Tao A, Jiang H, et al. Simultaneous real-time imaging of the ocular anterior segment including the ciliary muscle during accommodation. *Biomed Opt Express.* 2013;4:466-480.
 29. Fan R, He T, Qiu Y, Di YL, Xu SY, Li YY. Comparison of wavefront aberrations under cycloplegic, scotopic and photopic conditions using WaveScan. *Arq Bras Oftalmol.* 2012;75:116-121.
 30. Benozzi G, Leiro J, Facal S, Perez C, Benozzi J, Orman B. Developmental changes in accommodation evidenced by an ultrabiomicroscopy procedure in patients of different ages. *Med Hypothesis Discov Innov Ophthalmol.* 2013;2:8-13.
 31. Chin SS, Hampson KM, Mullen E. Role of ocular aberrations in dynamic accommodation control. *Clin Exp Optom.* 2009;92:227-237.
 32. Plainis S, Ginis HS, Pallikaris A. The effect of ocular aberrations on steady-state errors of accommodative response. *J Vis.* 2005;5(5):7.
 33. Gamba E, Sawides L, Dorronsoro C, Marcos S. Accommodative lag and fluctuations when optical aberrations are manipulated. *J Vis.* 2009;9(6):4.
 34. Wagner S, Conrad F, Bakaraju RC, Fedtke C, Ehrmann K, Holden BA. Power profiles of single vision and multifocal soft contact lenses. *Cont Lens Anterior Eye.* 2015;38:2-14.
 35. Shi Y, Queener HM, Marsack JD, Ravikumar A, Bedell HE, Applegate RA. Optimizing wavefront-guided corrections for highly aberrated eyes in the presence of registration uncertainty. *J Vis.* 2013;13(7):8.
 36. Lopez-Gil N, Martin J, Liu T, Bradley A, Diaz-Munoz D, Thibos LN. Retinal image quality during accommodation. *Ophthalmic Physiol Opt.* 2013;33:497-507.
 37. Li YJ, Choi JA, Kim H, Yu SY, Joo CK. Changes in ocular wavefront aberrations and retinal image quality with objective accommodation. *J Cataract Refract Surg.* 2011;37:835-841.
 38. Stachs O, Martin H, Behrend D, Schmitz KP, Guthoff R. Three-dimensional ultrasound biomicroscopy, environmental and conventional scanning electron microscopy investigations of the human zonula ciliaris for numerical modelling of accommodation. *Graefes Arch Clin Exp Ophthalmol.* 2006;244:836-844.
 39. Liu S, Datta A, Ho D, Dwelle J, et al. Effect of image registration on longitudinal analysis of retinal nerve fiber layer thickness of non-human primates using optical coherence tomography (OCT). *Eye Vis (Lond).* 2015;2:3.
 40. Lang A, Carass A, Al-Louzi O, et al. Combined registration and motion correction of longitudinal retinal OCT data. *Proc SPIE Int Soc Opt Eng.* 2016;9784.
 41. Enright JT. Ocular translation and cyclotorsion due to changes in fixation distance. *Vision Res.* 1980;20:595-601.
 42. Buehren T, Collins MJ, Loughridge J, Carney LG, Iskander DR. Corneal topography and accommodation. *Cornea.* 2003;22:311-316.